2022 30th Mediterranean Conference on Control and Automation (MED)
June 28 - July 1, 2022. Athens, Greece

2022 30th Mediterranean Conference on Control and Automation (MED) | 978-1-6654-0673-4/22/$31.00 ©2022 IEEE | DOI: 10.1109/MED54222.2022.9837261

Optimal MmWave Sensor Selection for Bearing-Only Localization in Smart Environments

Evangelos Vlachos[1], Evangelos D. Spyrou[2], Chrysostomos Stylios[1] and Kostas Berberidis[3]

***Abstract*— Nowdays, millimeter wave (mmWave) direction sensors are being used increasingly as general-purpose radars, since they can provide high-level of accuracy for a variety of situations at low-cost. Via mutliple mmWave sensors, bearing estimation can be derived to track the position of a target, while in smart environments several sensors can be deployed. In this work, we provide an optimal sensor selection technique, for choosing which sensors to activate for bearing estimation and which not. The proposed approach is decomposed into training phase, where sensor selection is performed, and operational phase, where bearing estimation is obtained. Via simulation results we evaluate the proposed approach compared with the conventional methodology of utilizing all available data streams.**

I. Introduction

Collaboration between humans and robots plays a significant role in smart industries since it helps to achieve improved production and efficiency. However, as the separation between robot and human workstations is removed, this evolution means breaking with established safety procedures [1]. Sensor nodes are used in industrial operations to collect system measurements. In [2], Hardware-In-the-Loop (HIL) technique is utilized to test a systematic sensor selection framework for control design.

The rough and dynamic nature of an industrial environment is characterized by multiple individuals and items moving and changing places, thus making sensing and tracking human position in such surroundings a difficult task. For object/body localization, a variety of sensors can be used, including acoustic/ultrasonic [3], vision [4], thermal [5], and radar [6] sensors. Of course, every situation is unique. The Human Activity Recognition (HAR) can be undertaken using wearable devices [7], [8], which are based on contact and device-free HAR [9], [10].

Usually vision based sensors provide a very informative representation of a scene acquisition in general; however, challenges can emerge such as their dependence on external illuminating scenes with poorness affecting rendering. This can have negative results with significant consequences, as for example, the Uber self-driving crash incident in Arizona at night conditions and the Tesla's autopilot testing which failed to detect the white side of a tractor trailer in bright sky, as we read in [11] and references therein. Furthermore, due to the camera's intrusive nature, privacy is also a major concern.

Other work exhibited that less information-rich ambient sensors can efficiently infer activities of humans; meanwhile they do not put subjects to security risks using RF signals. As we can see in [12] and references therein, Wi-Fi routers can be used when a human has fallen, which can find applications to the elderly or factory worker monitoring. However, this method is not robust enough. Wi-Fi has narrow band and does not offer enough range resolution to classify activities with robustness.

Radars, on the other hand, describe the scene using RF intensity-based spatial heat-maps, rather than vision-based sensors. Radars and other RF-based sensors employ their own signals to illuminate the target (active sensing), making them operationally resilient to scene illumination and weather. Even though RF sensing can accomplish great performance in HAR, it exhibits two major weaknesses. RF sensing needs high volume of training data to re-train its model in the case that the scene has been altered. In addition, the human is not in a place to recognise a number of activities by intuition from RF sensor data, as opposed to camera based modules [13].

Automotive radars using mmWave technology [14] are low-power and incredibly easy to deploy, often used in driveless vehicle applications. Moreover, higher operating bandwidths also enable mmWave radars to approximate the motion of the human body [15], [16]; thus making this technology significant for human tracking in industrial settings, where the conditions may be harsh due to the environment.

For automotive applications, typical mmWave sensors employ frequencies between 76 and 81 GHz, or frequencies around 60 GHz (e.g., 57 to 64 GHz following the European standard) as general-purpose short-range radars. mmWave radars are non-intrusive radars and can detect in a variety of conditions, such as darkness, smoke, and fog. mmWave radars do not increase cost as other sensors do, such as high resolution cameras. Although mmWave radars do not provide the same level of detail as a camera, they do offer high-resolution distance, velocity, and angle impression of the objects within a scene, which can be useful for determining their condition and motion as well as separating the object of interest from background noise. However, mmWave radars exhibit a fast attenuation and are prone to noise. Hence, the HAR is a challenging task using the mmWave radars [17].

In this work, we address the problem of optimal sensor selection for bearing estimation. Note that in harsh conditions the erroneous estimates of some sensors may affect

[1]Industrial Systems Institute, Athena Research and Innovation Centre, Greece {evlachos, stylios}@isi.gr
[2] Dept. of Informatics and Telecommunications, University of Ioannina, Greece e.spyrou@uoi.gr
[3] Dept. of Computer Engineering and Informatics, University of Patras, Greece berberid@ceid.upatras.gr

significantly the whole HAR process, therefore a technique for selecting the most reliable sensors would be desirable. To do so, we consider that all sensors are able to measure the angle of the impinging waves, and these angles are used to track the position of humans. The sensor selection problem is expressed as a sparse optimization one, and publicly available tools for convex optimization are employed. The relation between angle measurements and location follows a non-linear model, thus, we employ a pseudo-linear problem transformation. Simulation results demonstrate an optimal selection strategy for heterogeneous sensors, increases the localisation accuracy and hence the safety in smart environments with several available sensors.

II. Background

A. Millimeter wave direction sensors

The recent shift towards the millimeter-wave (mmWave) spectrum ($>$ 30 GHz) for radars enables highly precise range estimates to targeted objects, due to the high bandwidth available in these frequency bands. Furthermore, the reduced wavelength enables the application of small-sized massive antenna arrays, allowing to precisely scan the environment and to resolve the angular domain with high directionality. These inherent properties of mmWave radar systems and the recent availability of small and low-cost single-chip radar solutions operating in the mmWave band enabled plenty of new applications, such as human motion monitoring [16], vital signs monitoring [18], unmanned aerial vehicle pursuit [19], gesture recognition [20], as well as radar for autonomous cars [21], [22].

The basic principle of a radar is to transmit electromagnetic waves and to measure the signal reflected by objects (echo signal) to determine their range, velocity, and angle. Assuming a planar wavefront, one can relate the phase difference $\Delta\phi_m$ at the receive antennas of the m-th sensor, with the *measured* AoA as follows:

$$\theta_m = \arcsin \frac{\lambda \Delta\phi_m}{2\pi\delta}, \tag{1}$$

where λ is the wavelength, δ is the antenna spacing. Therefore, measuring the different phases of the individual receiving antennas of the antenna array of each sensor, the AoA measurements can be obtained. Moreover, recall that the AoA can be expressed based on the position at the Cartesian coordinates system of the m-th sensor $(a_{m,1}, a_{m,2})$, and the target (x_1, x_2) as follows:

$$h_m(x_1, x_2) = \arctan \frac{x_2 - a_{m,2}}{x_1 - a_{m,1}}. \tag{2}$$

B. Linerization of the system model

Let us consider that the noisy AoA measurements are given by the non-linear model:

$$\tilde{\theta}_m = h_m(\mathbf{x}) + n_m, \ m = 1, \ldots, M, \tag{3}$$

where M is the number of sensors, $h_m(\mathbf{x}) = \arctan \frac{x_2 - a_{m,2}}{x_1 - a_{m,1}}$, $\mathbf{x} = \begin{bmatrix} x_1, & x_2 \end{bmatrix}^T$, $n_m \sim \mathcal{N}(0, \sigma_n^2)$ is the additive white Gaussian noise (AWGN), which represents the sensor noise.

To cope with the non-linearity of the model, a *pseudolinear* equation can be devised by grouping the nonlinearities into the noise term. Thus, from (3) we have

$$\tilde{\theta}_m - n_m = \arctan \frac{x_2 - a_{m,2}}{x_1 - a_{m,1}} \Rightarrow \frac{\sin(\tilde{\theta}_m - n_m)}{\cos(\tilde{\theta}_m - n_m)} = \frac{x_2 - \alpha_{m,2}}{x_1 - \alpha_{m,1}}$$

$$\Rightarrow \begin{cases} \cos(\tilde{\theta}_m - n_m) = x_1 - \alpha_{m,1} \\ \sin(\tilde{\theta}_m - n_m) = x_2 - \alpha_{m,2} \end{cases}, \tag{4}$$

where using the standard trigonometric identities, we construct the following equivalent system of equations in matrix form:

$$\begin{bmatrix} \cos\tilde{\theta}_m & \sin\tilde{\theta}_m \\ \sin\tilde{\theta}_m & -\cos\tilde{\theta}_m \end{bmatrix} \begin{bmatrix} \cos n_m \\ \sin n_m \end{bmatrix} = \begin{bmatrix} x_1 \\ x_2 \end{bmatrix} - \begin{bmatrix} \alpha_{m,1} \\ \alpha_{m,2} \end{bmatrix}.$$

Next, we introduce the error vector $\boldsymbol{\xi}_m \in \mathbb{R}^{2\times 1}$, expressed as:

$$\boldsymbol{\xi}_m = \mathbf{A}_m^T \mathbf{x} - \mathbf{A}_m^T \boldsymbol{\alpha}_m, \tag{5}$$

where $\mathbf{A} \triangleq \begin{bmatrix} \cos\tilde{\theta}_m & \sin\tilde{\theta}_m \\ \sin\tilde{\theta}_m & -\cos\tilde{\theta}_m \end{bmatrix}$, $\boldsymbol{\xi}_m \triangleq \begin{bmatrix} \cos n_m \\ \sin n_m \end{bmatrix}$, $\boldsymbol{\alpha}_m \triangleq \begin{bmatrix} \alpha_{m,1} \\ \alpha_{m,2} \end{bmatrix}$, and $\mathbf{A}^T\mathbf{A} = \mathbf{I}$. Putting together the errors for all sensors $\boldsymbol{\xi} = [\boldsymbol{\xi}_1, \boldsymbol{\xi}_2, ..., \boldsymbol{\xi}_M]^T$, we obtain

$$\boldsymbol{\xi} = \mathbf{A}\mathbf{x} - \mathbf{h},$$

with $\mathbf{A} = [\mathbf{A}_1, \mathbf{A}_2, ..., \mathbf{A}_M]^T$ and $\mathbf{h} = [\boldsymbol{\alpha}_1^T \mathbf{A}_1, \boldsymbol{\alpha}_2^T \mathbf{A}_2, ..., \boldsymbol{\alpha}_K^T \mathbf{A}_K]^T$ the measurement matrix and vector respectively.

Therefore, the minimization is performed over the transformed noise space,

$$\min_{\mathbf{x}} \|\boldsymbol{\xi}\|^2 \text{ subject to } \boldsymbol{\xi} = \mathbf{A}\mathbf{x} - \mathbf{h}, \tag{6}$$

and the position estimate $\hat{\mathbf{x}}$ can be acquired by the least-squares estimation, i.e., $\hat{\mathbf{x}} = (\boldsymbol{A}^T\boldsymbol{A})^{-1}\mathbf{A}^T\mathbf{h}$.

C. Sensor selection

Consider the scenario where all sensors are able to transmit their measurements to a central station, where the solution of (6) is performed. The central station is able to control which sensors will be active and transmit their measurements and which not. Mathematically, the selection of the active/inactive sensors, and essentially, the subset of measurements $\mathbf{x}$, can be expressed using a binary vector $\mathbf{w} \in \{0, 1\}^{M\times 1}$. Specifically, $\mathbf{x}_w = \mathbf{W}\mathbf{x}$, where $\mathbf{W} = \text{diag}(\mathbf{w})$, with $\text{diag}(\cdot)$ places the input vector on the main diagonal. The aim of sensor selection is to obtain the best subset of measurements so as to minimize the estimation error, expressed using the error covariance matrix $\mathbf{E}(\mathbf{w})$, which is defined as: $\mathbf{E}(\mathbf{w}) = \mathcal{E}\{(\mathbf{x}_w - \hat{\mathbf{x}}_w)(\mathbf{x}_w - \hat{\mathbf{x}}_w)^H\}$, where $\mathcal{E}\{\cdot\}$ represents the expectation function.

To evaluate the estimation error, different functions $f(\mathbf{E}(\mathbf{w})$ can be used, and the typical choices for are: (i) *A-optimality*: minimizes the sum of eigenvalues of $\mathbf{E}$ with $f(\mathbf{E}(\mathbf{w}) \triangleq \text{tr}(\mathbf{E}(\mathbf{w})$, (ii) *E-optimality*: minimizes the maximum eigenvalue of $\mathbf{E}$ with $f(\mathbf{E}(\mathbf{w}) \triangleq \lambda_{\max}(\mathbf{E}(\mathbf{w}))$,

(iii) *D-optimality*: minimizes the determinant of $\mathbf{E}$ with $f(\mathbf{E}(\mathbf{w}) \triangleq \ln\det(\mathbf{E}(\mathbf{w}))$. Therefore, the following optimization problem can be constructed:

$$\arg \min_{\mathbf{w}\in\{0,1\}^K} f(\mathbf{E}(\mathbf{w})) \text{ subject to } \mathbf{1}_K^T\mathbf{w} = M, \quad (7)$$

where $f(\mathbf{E}(\mathbf{w})$ is a scalar cost function related to the error covariance matrix $\mathbf{E}$, while the constraint sets the number of active sensors M. The problem in (7) is a combinatorial optimization problem involving $\begin{pmatrix} K \\ M \end{pmatrix}$ searches.

III. Proposed Approach

A. Bearing measurements model

Bearing estimation is a target localization technique based only on bearing (angle) measurements from a set of direction finding sensors, such as mmWave radar sensors. Specifically, in cases with large antenna apertures (massive MIMO [23]), bearing estimation can provide accurate localization results even in multipath environments. However, distributed measurements may be subject to several impairments such as measurement noise and signal blockages, thereby dramatically reducing the localization performance. On this premise, we consider the selection of the subset of measurements which end up to the best estimation performance.

In vector form (3) can be written as:

$$\tilde{\boldsymbol{\theta}} = \mathbf{h}(\mathbf{x}) + \mathbf{n}, \quad (8)$$

where

$$\tilde{\boldsymbol{\theta}} \triangleq \left[\ \tilde{\theta}_1, \ldots, \tilde{\theta}_M\ \right]^T, \mathbf{n} = \left[\ n_1, \ldots, n_M\ \right]^T,$$

while $\mathbf{h}(\mathbf{x}) \triangleq \left[\ h_1(\mathbf{x}), \ldots, h_M(\mathbf{x})\ \right]^T$ is the non-linear bearing measurement function which depends on $\mathbf{x}$.

B. Cramer-Rao Lower Bound

Cramer-Rao Lower Bound (CRLB) provides the theoretical performance threshold for any unbiased estimator. Given that the estimator $\hat{\mathbf{x}}$ is unbiased (i.e. $\mathcal{E}\{\hat{\mathbf{x}}\} = \mathbf{x}$), the CRLB is expressed as:

$$\mathcal{E}\{(\mathbf{x} - \hat{\mathbf{x}})(\mathbf{x} - \hat{\mathbf{x}})^H\} \geq \mathbf{F}^{-1}(\mathbf{x}), \quad (9)$$

where $\mathbf{F} \in \mathbb{C}^{2\times 1}$ is the Fisher information matrix (FIM), expressed as:

$$\mathbf{F}(\mathbf{x}) = \sum_{m=1}^{M} \mathbf{F}_m(\mathbf{x}) \quad (10)$$

with

$$[\mathbf{F}_m]_{i,j} = \frac{1}{\sigma_n^2}\left(\frac{\partial h_m(\mathbf{x})}{\partial x_i}\right)^T\left(\frac{\partial h_m(\mathbf{x})}{\partial x_j}\right). \quad (11)$$

Specifically for our case, after obtaining the derivative of the function $h_m(\mathbf{x})$ over x_is, the FIM for the m-th sensor can be expressed as:

$$\mathbf{F}_m = \frac{1}{\sigma_n^2 d_m^2}\mathbf{P}(\mathbf{x} - \boldsymbol{\alpha}_m)(\mathbf{x} - \boldsymbol{\alpha}_m)^T\mathbf{P}^T, \quad (12)$$

Algorithm 1 Proposed algorithm for optimal sensor selection and bearing estimation

Input: $\boldsymbol{\alpha}_m$, $\mathbf{A}$, $\mathbf{h}$, σ_n^2, λ_e
Output: $\mathbf{W}$

1: Calculate FIM $\mathbf{F}_m$ via (12) for all sensors, $m = 1, 2, \ldots, M$.
2: Solve (17) and obtain $\tilde{\mathbf{w}}$.
3: Perform thresholding to $\tilde{\mathbf{w}}$ as in (18) to obtain the binary vector $\mathbf{w}$.
4: $\mathbf{W} = \text{diag}(\mathbf{w})$.

where $\mathbf{P} = \begin{bmatrix} 1 & -1 \\ -1 & 1 \end{bmatrix}$. In this work, the minimum eigenvalue constraint is utilized as a performance measure, i.e.,

$$\lambda_{\min}(\mathbf{F}) \geq \lambda_e, \quad (13)$$

where threshold λ_e describes the predefined estimator.

C. Sensor selection problem formulation

To proceed, let us express the FIM when sensor selection is performed. Specifically, given that w_m is the m-th component of the binary vector $\mathbf{w}$, then

$$\mathbf{F}(\mathbf{w}, \mathbf{x}) = \sum_{m=1}^{M} w_m\mathbf{F}_m. \quad (14)$$

Thus, when the m-th sensor is active ($w_m = 1$), it contributes to the FIM by adding the term $\mathbf{F}_m$ to the overall sum. Subsequently, the minimum eigenvalue of FIM depends on which measurements are taken into account, and the inequality constrained is now expressed as:

$$\lambda_{\min}(\mathbf{F}(\mathbf{w}, \mathbf{x})) \geq \lambda_e. \quad (15)$$

The inequality in (15) can be expressed as the following linear matrix inequality (LMI):

$$\sum_{m=1}^{M} w_m\mathbf{F}_m - \lambda_e\mathbf{I} \succeq \mathbf{0}, \quad (16)$$

which essentially sets a lower bound on each eigenvalue of matrix $\mathbf{F}(\mathbf{w}, \mathbf{x})$.

The problem (7) can be approximated by a semi-convex one, relaxing the binary constraint on $\mathbf{w}$ by the convex box constraint $\tilde{\mathbf{w}} \in [0, 1]^M$ [24]. Thus, the proposed problem formulation takes the following expression

$$\min_{\tilde{\mathbf{w}}\in[0,1]^M} \|\tilde{\mathbf{w}}\|_1 \quad \text{subject to} \quad \sum_{m=1}^{M} \tilde{w}_m\mathbf{F}_m - \lambda_e\mathbf{I} \succeq \mathbf{0}, \quad (17)$$

where $\|\tilde{\mathbf{w}}\|_1 = \sum_{m=1}^{M} |w_m|$ denotes the ℓ_1-norm. The optimization problem (17) is a standard semi-definite problem in the inequality form, which can be efficiently solved in polynomial time using interior-point methods. Implementations of interior-point methods are publicly available in the form of well-known toolboxes like Yalmip [25], SeDuMi [26], and CVX [27].

The overall proposed algorithm for obtaining $\mathbf{W}$ is summarized in Algorithm 1. Note that, the solution of (17) returns the sparse vector $\tilde{\mathbf{w}}$ with entries of real values in $[0, 1]$. Thresholding these values is required in order to determine the active/inactive sensors. Specifically, thresholding operation is described as:

$$w_m = \begin{cases} 1 & \text{if } \tilde{w}_m > \gamma \\ 0 & \text{otherwise.} \end{cases} \tag{18}$$

IV. Numerical Results

In this section, we demonstrate the effectiveness of the proposed approach, when several mmWave sensors have been deployed in a smart industrial environment, to sense the presence of human bodies via bearing estimation. To do so, low-cost industrial mmWave sensors could be employed, such as IWR1443 [28], which can detect human bodies up to 40m with 120° Field of View. We assume that these sensors transmit their measurements into a central station, where the processing is performed in order to monitor the human position for their safety. The overall approach is composed by two phases, namely *training and operational phase*, as shown in Fig. 1. During the training phase, the optimal selection algorithm is executed, and the subset of active sensors are determined. During the operational phase, the obtained subset of active sensors transmit their measurements to the central station, where bearing estimation is performed.

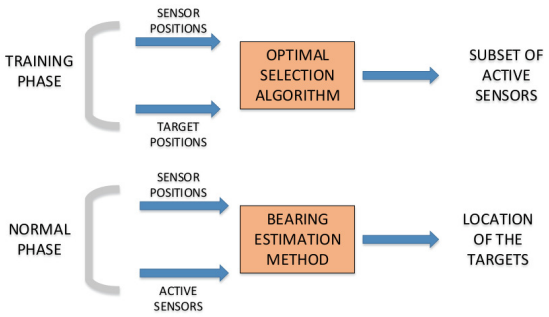

Fig. 1: Illustration of the proposed two-phase approach.

For simplicity, let us consider a two-dimensional grid area, where M sensors can be placed on points denoted by the 2×1 vector $\boldsymbol{\alpha}_m = [a_{m,1}, a_{m,2}]^T$, with $m = 1, 2, \ldots, M$. In Fig. 2, we give an example for $M = 32$ sensors placed uniformly on the edges of a rectangular, while in Fig. 3 the case of randomly placed sensors on an 8×8 grid. In both cases, the target is placed at the position $(5, 5)$. To proceed, let us assume that one target is located in the specific area, where its position is unknown and denoted by $\mathbf{x} = [x_1, x_2]^T$, while $d_m = \|\mathbf{x} - \boldsymbol{\alpha}_m\|_2$ denotes the pairwise distance between the target and the m-th sensor.

During the training phase, the sensor and target positions are considered known, thus, Algorithm 1 is employed to select the optimal subset of sensors to activate for the upcoming operational phase. The output of Algorithm 1 is the diagonal matrix $\mathbf{W}$ with $[\mathbf{W}]_{k,k} \in [0, 1]$ for $k = 1, 2, \ldots, M$. In Figs. 4 and 5 we plot the results of Algorithm 1 for the cases

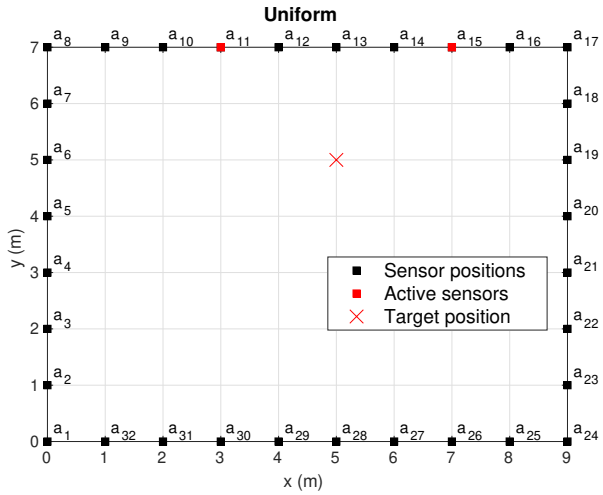

Fig. 2: Uniformly placed sensors.

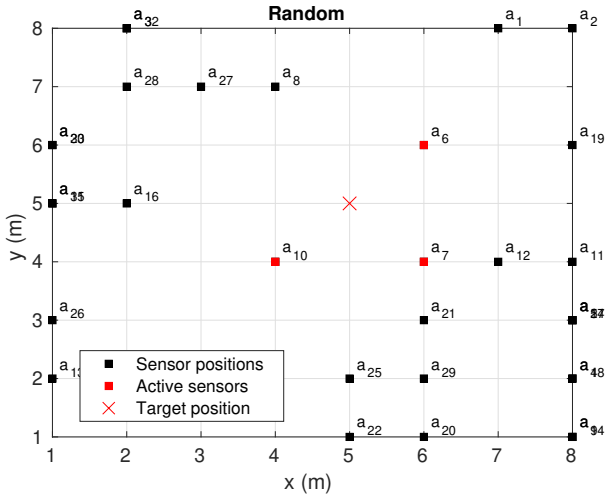

Fig. 3: Randomly placed sensors.

of uniform and random sensor placement. Along with the outputs of Algorithm 1, we also plot the non-thresholded values $\tilde{\mathbf{W}}$.

Next, for the operational phase, the selected sensors transmit their measurements to the central processing unit. There, we obtain the bearing estimation in order to find the location of the target. For comparison, we also evaluate the bearing estimation utilizing the measurements from all sensors. To proceed, let us define the Mean-Square-Error (MSE) of the bearing estimation as:

$$\text{MSE} = \frac{\|\mathbf{x} - \hat{\mathbf{x}}\|}{\|\mathbf{x}\|}, \tag{19}$$

and the Signal-to-Noise-Ratio (SNR) as:

$$\text{SNR} = \frac{1}{\sigma_n^2 M d_m} \tag{20}$$

Thus, in Fig. 6 the MSE is plotted versus the SNR for three cases of the number of sensors M. The proposed technique

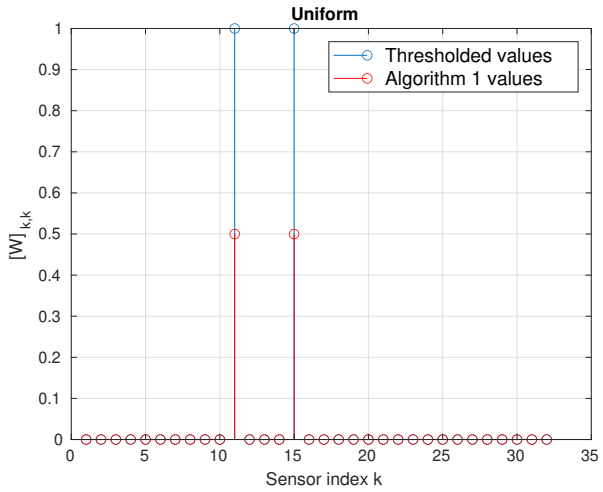

Fig. 4: Subset of selected sensors for uniform placement.

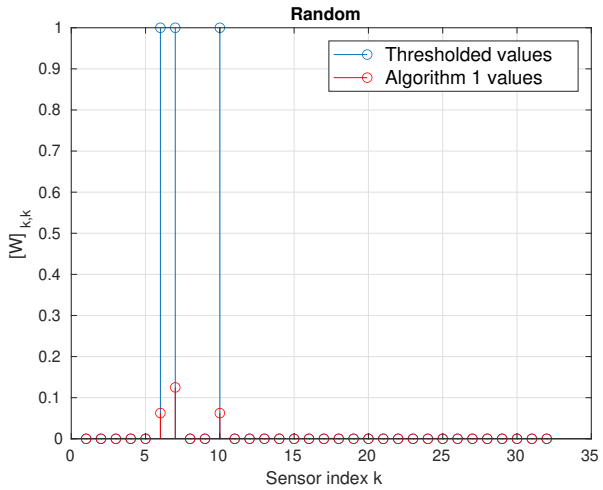

Fig. 5: Subset of selected sensors for random placement.

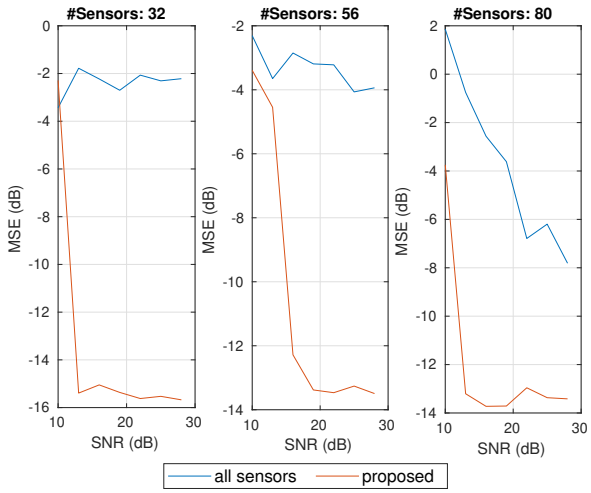

Fig. 6: Performance comparisons during operational phase over SNR for uniform sensor placement.

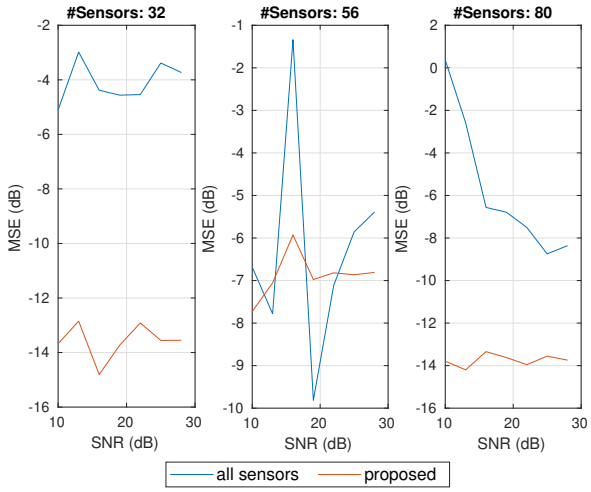

Fig. 7: Performance comparisons during operational phase over SNR for random sensor placement.

exhibits lower MSE as the SNR increases, for all cases of M. Therefore, it is beneficial to select a subset of active sensors than capturing measurements from all available sensors for the considered SNR range. Fig. 7 shows the case of random sensor placement, where a similar behaviour is observed, with the proposed technique achieving much lower MSE than the conventional approach.

Next we evaluate the impact of the number of the available sensors M to the performance of the proposed approach. To do so, first during the training phase the subset of sensors is selected for each case of M, and then during the operational phase the bearing estimation is performed. In Fig. 8 (left) the MSE over the number of available sensors M is plotted for uniform sensor placement, while in Fig. 8 (right) for random sensor placement. The number on the curve points indicate the number of the active sensors. It is evident that the number of available sensors changes the output of the selection algorithm, note however that in all cases the position of the target is at the position $(5, 5)$. Thus, the variation on the MSE over M is due to the different sensors that are being selected at each case.

V. Conclusion

In this paper, we investigated the problem of optimal sensor selection for the estimation of bearing. To that end, we considered that the sensors have the capability to measure the angle of the impinging waves. The problem is formulated in terms of sparse optimisation and convex optimisation methods were used. A pseudo-linear problem formulation was devised, since the angle measurements and the location adhere to a non-linear model. In the simulation results, two cases have been examined, namely uniform and random placement of the sensors on a grid. Algorithm 1, that has been devised, selected the optimal subset of sensors, which

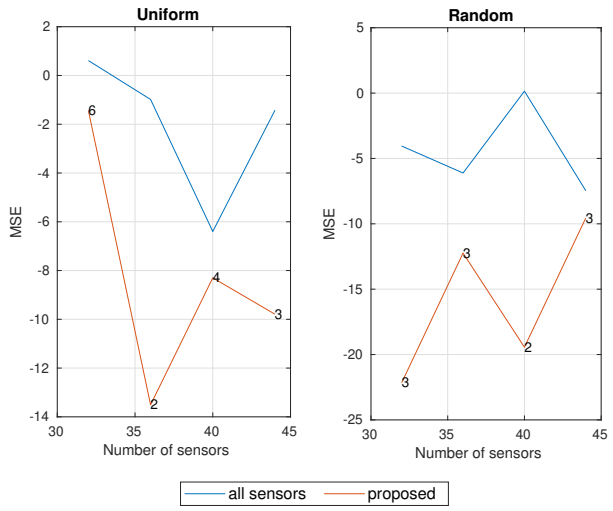

Fig. 8: Performance comparisons during operational phase over the number of available sensors for uniform sensor placement (left) and random sensor placement (right).

are activated to be used in the operational phase. Thereafter, a comparison between the proposed method and the measurements from all sensors has been undertaken, with the proposed method exhibiting lower MSE with the increase of the SNR. Uniform and random placement of sensors have been evaluated, showing a change in the result of the selection algorithm and the fact that the target is found to be in the position of the assumption.

REFERENCES

[1] S. Robla-Gómez, V. M. Becerra, J. R. Llata, E. González-Sarabia, C. Torre-Ferrero, and J. Pérez-Oria, "Working together: A review on safe human-robot collaboration in industrial environments," *IEEE Access*, vol. 5, pp. 26 754–26 773, 2017.

[2] K. M. Deliparaschos, K. Michail, S. G. Tzafestas, and A. C. Zolotas, "A model-based embedded control hardware/software co-design approach for optimized sensor selection of industrial systems," in *2015 23rd Mediterranean Conference on Control and Automation (MED)*, 2015, pp. 889–894.

[3] A. Wang and S. Gollakota, "Millisonic: Pushing the limits of acoustic motion tracking," in *Proceedings of the 2019 CHI Conference on Human Factors in Computing Systems*, 2019, pp. 1–11.

[4] Y. Xiao, V. R. Kamat, and C. C. Menassa, "Human tracking from single rgb-d camera using online learning," *Image and Vision Computing*, vol. 88, pp. 67–75, 2019.

[5] S. A. Manssor, Z. Ren, R. Huang, and S. Sun, "Human activity recognition in thermal infrared imaging based on deep recurrent neural networks," in *2021 14th International Congress on Image and Signal Processing, BioMedical Engineering and Informatics (CISP-BMEI)*. IEEE, 2021, pp. 1–7.

[6] F. Zoghlami, O. K. Sen, H. Heinrich, G. Schneider, E. Ercelik, A. Knoll, and T. Villmann, "ToF/Radar early feature-based fusion system for human detection and tracking," in *2021 22nd IEEE International Conference on Industrial Technology (ICIT)*, vol. 1. IEEE, 2021, pp. 942–949.

[7] H. Truong, S. Zhang, U. Muncuk, P. Nguyen, N. Bui, A. Nguyen, Q. Lv, K. Chowdhury, T. Dinh, and T. Vu, "Capband: Battery-free successive capacitance sensing wristband for hand gesture recognition," in *Proceedings of the 16th ACM Conference on Embedded Networked Sensor Systems*, 2018, pp. 54–67.

[8] I. Khokhlov, L. Reznik, J. Cappos, and R. Bhaskar, "Design of activity recognition systems with wearable sensors," in *2018 ieee sensors applications symposium (sas)*. IEEE, 2018, pp. 1–6.

[9] X. Liu, P. Ghosh, O. Ulutan, B. Manjunath, K. Chan, and R. Govindan, "Caesar: cross-camera complex activity recognition," in *Proceedings of the 17th Conference on Embedded Networked Sensor Systems*, 2019, pp. 232–244.

[10] W. Jiang, C. Miao, F. Ma, S. Yao, Y. Wang, Y. Yuan, H. Xue, C. Song, X. Ma, D. Koutsonikolas *et al.*, "Towards environment independent device free human activity recognition," in *Proceedings of the 24th Annual International Conference on Mobile Computing and Networking*, 2018, pp. 289–304.

[11] A. Sengupta, F. Jin, R. Zhang, and S. Cao, "mm-pose: Real-time human skeletal posture estimation using mmwave radars and cnns," *IEEE Sensors Journal*, vol. 20, no. 17, pp. 10 032–10 044, 2020.

[12] A. D. Singh, S. S. Sandha, L. Garcia, and M. Srivastava, "Radhar: Human activity recognition from point clouds generated through a millimeter-wave radar," in *Proceedings of the 3rd ACM Workshop on Millimeter-wave Networks and Sensing Systems*, 2019, pp. 51–56.

[13] S. Ding, Z. Chen, T. Zheng, and J. Luo, "RF-net: A unified meta-learning framework for RF-enabled one-shot human activity recognition," in *Proceedings of the 18th Conference on Embedded Networked Sensor Systems*, 2020, pp. 517–530.

[14] J. Hasch, E. Topak, R. Schnabel, T. Zwick, R. Weigel, and C. Waldschmidt, "Millimeter-wave technology for automotive radar sensors in the 77 ghz frequency band," *IEEE transactions on microwave theory and techniques*, vol. 60, no. 3, pp. 845–860, 2012.

[15] F. Jin, R. Zhang, A. Sengupta, S. Cao, S. Hariri, N. K. Agarwal, and S. K. Agarwal, "Multiple patients behavior detection in real-time using mmwave radar and deep cnns," in *2019 IEEE Radar Conference (RadarConf)*. IEEE, 2019, pp. 1–6.

[16] R. Zhang and S. Cao, "Real-time human motion behavior detection via cnn using mmwave radar," *IEEE Sensors Letters*, vol. 3, no. 2, pp. 1–4, 2019.

[17] H. Cui and N. Dahnoun, "High precision human detection and tracking using millimeter-wave radars," *IEEE Aerospace and Electronic Systems Magazine*, vol. 36, no. 1, pp. 22–32, 2021.

[18] M. Alizadeh, G. Shaker, J. C. M. De Almeida, P. P. Morita, and S. Safavi-Naeini, "Remote monitoring of human vital signs using mm-wave FMCW radar," *IEEE Access*, vol. 7, pp. 54 958–54 968, 2019.

[19] S. Dogru and L. Marques, "Pursuing drones with drones using millimeter wave radar," *IEEE Robotics and Automation Letters*, vol. 5, no. 3, pp. 4156–4163, 2020.

[20] K. A. Smith, C. Csech, D. Murdoch, and G. Shaker, "Gesture recognition using mm-wave sensor for human-car interface," *IEEE sensors letters*, vol. 2, no. 2, pp. 1–4, 2018.

[21] N. C. Iyer, P. Pillai, K. Bhagyashree, V. Mane, R. M. Shet, P. Nissimagoudar, G. Krishna, and V. Nakul, "Millimeter-wave AWR1642 radar for obstacle detection: autonomous vehicles," in *Innovations in Electronics and Communication Engineering*. Springer, 2020, pp. 87–94.

[22] T. Zhou, M. Yang, K. Jiang, H. Wong, and D. Yang, "MMW radar-based technologies in autonomous driving: A review," *Sensors*, vol. 20, no. 24, p. 7283, 2020.

[23] N. Garcia, H. Wymeersch, E. G. Larsson, A. M. Haimovich, and M. Coulon, "Direct localization for massive MIMO," *IEEE Transactions on Signal Processing*, vol. 65, no. 10, pp. 2475–2487, 2017.

[24] S. P. Chepuri and G. Leus, "Sparsity-promoting sensor selection for non-linear measurement models," *IEEE Transactions on Signal Processing*, vol. 63, no. 3, pp. 684–698, 2015.

[25] J. Lofberg, "YALMIP: A toolbox for modeling and optimization in MATLAB," in *2004 IEEE international conference on robotics and automation (IEEE Cat. No. 04CH37508)*. IEEE, 2004, pp. 284–289.

[26] J. F. Sturm, "Using SeDuMi 1.02, a MATLAB toolbox for optimization over symmetric cones," *Optimization methods and software*, vol. 11, no. 1-4, pp. 625–653, 1999.

[27] M. Grant, S. Boyd, and Y. Ye, "CVX users' guide," in *Tech. Rep. Build*. Cambridge Univ., 2009, p. 711.

[28] Texas Instruments, "IWR1443 Single-Chip 76- to 81-GHz mmWave Sensor." [Online]. Available: https://www.ti.com/lit/ds/symlink/iwr1443.pdf?ts=1651673300572, (retrieved 5th of May 2022)